Chinese Journal of Natural Medicines

Quercetin reverses the breast cancer–promoting effects of depression by targeting PPAR γ

Yingchao Wu, Yuqi Liang, Liushan Chen, Jieting Chen, Junfeng Huang, Congwen Yang, Qian Zuo, Qianjun Chen

Citation: Yingchao Wu, Yuqi Liang, Liushan Chen, Jieting Chen, Junfeng Huang, Congwen Yang, Qian Zuo, Qianjun Chen, Quercetin reverses the breast cancer–promoting effects of depression by targeting PPAR γ , Chinese Journal of Natural Medicines, 2026, 24(11), 1310–1321. doi: 10.1016/S1875–5364(26)61222–8.

View online: https://doi.org/10.1016/S1875–5364(26)61222–8

Related articles that may interest you

Paeoniflorin alleviates depression by inhibiting the activation of NLRP3 inflammasome *via* promoting mitochondrial autophagy

Chinese Journal of Natural Medicines. 2024, 22(6), 515–529 https://doi.org/10.1016/S1875–5364(24)60654–0

Hepatic metabolomics combined with network pharmacology to reveal the correlation between the anti–depression effect and nourishing blood effect of Angelicae Sinensis Radix

Chinese Journal of Natural Medicines. 2023, 21(3), 197–213 https://doi.org/10.1016/S1875–5364(23)60421–2

Ginkgo biloba extract protects against depression–like behavior in mice through regulating gut microbial bile acid metabolism

Chinese Journal of Natural Medicines. 2023, 21(10), 745–758 https://doi.org/10.1016/S1875–5364(23)60496–0

The thalamic–primary auditory cortex circuit: a pathway to resilience in the face of stress and a potential target for depression treatment

Chinese Journal of Natural Medicines. 2023, 21(11), 801–802 https://doi.org/10.1016/S1875–5364(23)60447–9

Design, synthesis, and biological evaluation of novel chrysin derivatives as poly(ADP–ribose) polymerase 1 (PARP1) inhibitors for the treatment of breast cancer

Chinese Journal of Natural Medicines. 2024, 22(5), 455–465 https://doi.org/10.1016/S1875–5364(24)60642–4

Oroxyloside protects against dextran sulfate sodium–induced colitis by inhibiting ER stress *via* PPAR γ activation

Chinese Journal of Natural Medicines. 2024, 22(4), 307–317 https://doi.org/10.1016/S1875–5364(24)60615–1

Wechat

Chinese Journal of Natural Medicines 24 (2026) 1310-1321

Contents lists available at ScienceDirect

Chinese Journal of Natural Medicines

journal homepage: www.cjnmcpu.com/



Original article

Quercetin reverses the breast cancer-promoting effects of depression by targeting PPARγ

Yingchao Wu[a, b, c, d, e, Δ], Yuqi Liang[a, b, c, e, Δ], Liushan Chen[a, b, c], Jieting Chen[a, c], Junfeng Huang[f], Congwen Yang[a, c, d], Qian Zuo[a, b, c, *], Qianjun Chen[a, b, c, *]

[a] *State Key Laboratory of Traditional Chinese Medicine Syndrome, The Second Affiliated Hospital of Guangzhou University of Chinese Medicine, Guangzhou 510006, China*
[b] *Chinese Medicine Guangdong Laboratory, Hengqin 519031, China*
[c] *Department of Breast Medicine, Guangdong Provincial Hospital of Chinese Medicine, Guangzhou 510006, China*
[d] *The Second Clinical College of Guangzhou University of Chinese Medicine, Guangzhou 510006, China*
[e] *Postdoctoral Research Center, Guangdong Provincial Hospital of Chinese Medicine, Guangzhou 510006, China*
[f] *The First Clinical College of Guangzhou University of Chinese Medicine, Guangzhou 510405, China*

ARTICLE INFO

Article history:
Received 23 February 2026
Revised 13 April 2026
Accepted 21 June 2026
Available online 20 November 2026

Keywords:
Breast cancer
Depression
PPARγ
Norepinephrine
Quercetin

ABSTRACT

Breast cancer (BC) has become the most prevalent cancer worldwide, and BC patients have the highest rate of depression of all cancer patients. However, previous studies, especially studies based on clinical sample data, have failed to reveal exactly how depression affects BC. Two-sample Mendelian randomization (TSMR) was used to determine the causal relationship between depression and BC. Transcriptomics and metabolomics were used to analyze BC samples from nondepressed and depressed patients and to validate differentially expressed genes and key metabolites *in vitro*. Molecular docking techniques were used to identify compounds that regulate key targets and validate the functions of the compounds in *in vitro* and *in vivo* animal models. Depression was identified as a risk factor for BC by the TSMR analysis. On the basis of clinical samples, for the first time, we identified PPARγ and norepinephrine (NE) as key genes and metabolites that mediate the pro-BC effects of depression. In addition, we demonstrated that quercetin can target PPARγ and reverse the procancer effects of PPARγ inhibition mediated by chronic stress in BC cells. Moreover, we found that PPARγ may be associated with the inhibition of $CD8^+$ T cells in the tumor immune microenvironment. In conclusion, depression can increase the infiltration level of NE in tumors and inhibit the expression of PPARγ in tumor cells, thus promoting the proliferation of BC cells and inhibiting the infiltration of $CD8^+$ T cells in the immune microenvironment, ultimately leading to accelerated tumor growth. Quercetin can target PPARγ and reverse this cancer-promoting process.

1. Introduction

The latest data show that breast cancer (BC) has become the most common malignant tumor in women and poses a serious threat to women's health [1]. Previous reports have divided the causes of BC into genetic factors, marital and reproductive history, and environmental factors [2, 3]. Among all types of cancer patients, the proportion and number of BC patients with depression are significantly greater than those with other types of cancer [4-6]. Researchers further confirmed that depression in patients was associated with a higher incidence of cancer, a poorer cancer prognosis, and greater cancer mortality [7]. Recent research also supports this theory, as most patients have a long history of negative emotions or exposure to stressful events before the onset of cancer [8, 9]. Our center previously conducted a meta-analysis of depression and survival prognosis in 282 203 patients with BC, and the results of multifactor analysis also revealed that depressive negative emotion was an independent risk factor for BC prognosis [10]. Despite the strong correlation between depression and BC, the molecular mechanism of the interaction between the two is still poorly understood, and basic research data based on clinical samples are currently not available in public databases. In previous studies on the relationship between depression and peripheral solid tumors, hyperactivation of the hypothalamic–pituitary–adrenal axis was shown to mediate the "neuroendocrine–immune" network to regulate tumor growth, which is a classic "central–peripheral tumor" mechanism [11]. Recent studies have also shown that continuous psychological stress can directly stimulate the sympathetic nervous system to continuously activate it, promote the release of stress hormones [including those in the noradrenal gland such as norepinephrine (NE)], and restrict the migration of $CD8^+$ T cells and their infiltration into tumors [12]. This process results in the desertification of $CD8^+$ T cells in the tumor immune microenvironment. However, these studies were all conducted in animal models, and there is no direct evidence from clinical samples.

The peroxisome proliferator-activated receptor (PPAR) superfamily is a member of a ligand-activated nuclear transcription factor superfamily divided into three subtypes: α, β/δ, and γ.

* Corresponding author.
E-mail addresses: 827649822@qq.com (Q. Zuo); cqj55@163.com (Q. Chen)
Δ These authors contributed equally to this work.

https://doi.org/10.1016/S1875-5364(26)61222-8
Copyright © 2026, China Pharmaceutical University. Published by Elsevier B.V. All rights are reserved.

PPARs play roles within the nucleus, regulate gene expression by binding to specific ligands, and are involved in a variety of biological processes. Studies have shown that the expression of PPARs is closely related to positive emotions, and a state of low mood results in significant inhibition of the expression of PPARγ [13]; however, whether this effect is related to the progression of cancer has not been reported. Interestingly, we reported that quercetin inhibits the progression of depressive BC but has no significant effect on nondepressive BC [14, 15].

Quercetin is a natural flavonol compound with high bioactivity from a wide range of sources, such as onion, black tea, guava and other plant-derived foods [16, 17]. In addition, many traditional Chinese medicines, such as *Sophora japonica* L. (Flos Sophorae) and *Bupleurum chinense* DC (Bupleuri Radix), also have a high content of quercetin. The United States FDA approved the extraction of quercetin from natural products on November 22, 2010. Japan and South Korea have also listed quercetin as a food additive. These data indicate that quercetin is highly safe and has the potential to become a drug [16].

In this study, we revealed differences in gene expression and metabolites in BC tissues from nondepressed and depressed patients on the basis of clinical samples and validated them *in vitro* and *in vivo* models. Furthermore, the above model was used to verify the effect of quercetin on depressive BC and its mechanism. Through this study, we propose a new mechanism by which depression promotes BC progression and provide a safe and effective intervention method.

2. Materials and methods

2.1. Clinical samples and animal ethics statement

Permission for the experimental scheme was obtained from the Ethics Committee of Guangdong Provincial Hospital of Chinese Medicine (Approval No. BF2019-120-04) and the Laboratory Animal Ethics Committee of Guangdong Province Hospital of Chinese Medicine (Approval No. 2022079, dates: September 22, 2022; and No. 2022008, dates: January 22, 2022). All patients provided written informed consent to participate in the study (Registration No. ChiCTR2200059811). This study utilized female C57BL/6J (n = 110) and BALB/c-nu (n = 40) mice (8 weeks old; body mass 17–19 g) obtained from a specific pathogen-free (SPF) certified provider (Beijing HFK Bioscience Co., Ltd., Beijing, China). All murine subjects were maintained in IVC systems under controlled environmental conditions: 24–26 °C ambient temperature, 50% ± 5% relative humidity, and 12/12-hour photoperiod regulation, with ad libitum access to autoclaved feed and water. Experimental protocols complied with national animal welfare regulations international guidelines. During the experiment, all the mice were randomly divided into 10 mice/groups.

2.2. Mendelian randomization (MR) study design

Our experimental design follows a general two-sample MR design [18]. We utilized depression as an exposure factor. A diagnosis of BC was considered the outcome of MR analysis. We obtained depression data (ukb-a-373) and BC data (ieu-b-4810) from the Integrative Epidemiology Unit GWAS database (https://gwas.mrcieu.ac.uk/). All analyses were conducted using the "TwoSampleMR" and "MR-PRESSO" packages in R version 4.2.2. The key parameters of this study are set as follows: (1) genome-wide significance level at $P < 5 \times 10^{-5}$; (2) linkage disequilibrium clustering ($r^2 < 0.001$, region size = 10 000 kb; and (3) F statistic > 10. Among these methods, the IVW method played a predominant role. The statistical significance threshold for evidence was set at $P < 0.05$.

2.3. Patient grouping and clinical tumor sample collection

BC patients were grouped before the operation according to the Hamilton Depression Scale (HAMD-17) and the Hamilton Anxiety Scale (HAMA). Patients with HAMD-17 scores greater than or equal to 7 points and HAMA scores greater than or equal to 7 points were considered to have depression. After the tumor tissue was removed during the operation, the tissue was rinsed with normal saline within 10 min *in vitro* to remove the blood stains and dirt on the surface of the tissue, and the tissue from nonstudy sites, such as adipose tissue, was removed. After the tissue was dried with sterile gauze, it was placed in a precooled cryogenic storage tube, frozen in liquid nitrogen, and stored in an ultralow-temperature refrigerator at −80 °C.

2.4. RNA sequencing

Total RNA was isolated from the samples using TRIzol reagent (Invitrogen). Subsequently, cDNA libraries were prepared from each RNA sample with the VAHTS Universal V6 RNA-seq Library Prep Kit for Illumina (Vazyme, Inc.), following the manufacturer's recommended protocols. The libraries were subjected to quality control with an Agilent 2200 instrument and sequenced by DNBSEQ-T7 on a 150 bp paired-end run. Before read mapping, clean reads were obtained from the raw reads by removing the adaptor sequences and low-quality reads. The clean reads were then aligned to the human genome (Ensemble 109) using the Star. HTseq was used to obtain gene counts, and the RPKM method was used to determine gene expression. Difference analysis and enrichment analysis were performed *via* OmicShare Tools [19], and survival curve and immune infiltration analyses were performed *via* the Xiantao Academic bioinformatics tool (www.xiantao.love).

2.5. Immunofluorescence (IF)

The frozen tissue was embedded in optimal cutting temperature (OCT) compound and cut into 10 μm slices, and the cells were scraped after NE (Cat. #HY-13715, MedChemExpress, Shanghai, China) or quercetin (Cat. #HY-18085, MedChemExpress) intervention for subsequent experiments. The slices were immunostained with anti-PPARγ (1 : 100, Cat. #2435, Cell Signaling Technology, Boston, USA) primary antibodies, followed by incubation with secondary antibodies (1 : 500, Cat. #4413, Cell Signaling Technology). All the slices were stained with DAPI to visualize the nuclei of the tissues. The slices were subsequently washed three times with Tris-buffered saline plus Tween-20 (TBST) solution, after which the red or green fluorescence intensity was measured using a fluorescence microscope to determine the protein content of each sample.

2.6. Western blotting (WB)

Briefly, fresh tumor tissues or cultured cells were homogenized in RIPA buffer. Following lysis, samples were centrifuged at 12 000 × g for 15 min (4 °C), and protein concentration in the resultant supernatant was quantified with an enhanced bicinchoninic acid assay kit (Cat. #P0010S, Beyotime Biotechnology, China). Equivalent protein amounts were resolved by SDS-PAGE and electrophoretically transferred onto PVDF membranes (Cat. #GVHP04700; Merck KGaA, Germany). Next, the PVDF membranes were blocked with TBST containing 5% skim milk for 1 h and incubated with the indicated primary antibodies, including anti-PPARγ (1 ∶ 1000, Cat. #2435, Cell Signaling Technology), anti-N-cadherin (1 ∶ 1000, Cat. #13116, Cell Signaling Technology), anti-E-cadherin (1 ∶ 1000, Cat. #3195, Cell Signaling Technology), anti-Bax (1 ∶ 1000, Cat. #2772, Cell Signaling Technology), anti-Bcl-2 (1 ∶ 1000, Cat. #15071, Cell Signaling Techno-

logy), anti-cleaved Caspase-3 (1 ∶ 1000, Cat. #9661, Cell Signaling Technology), and anti-GAPDH (1 ∶ 1000, Cat. #2118, Cell Signaling Technology), after which the membranes were incubated with the corresponding secondary antibodies (1 ∶ 8000) for 60 min at room temperature. The PVDF membranes were washed three times with TBST solution and visualized with a Beyotime hypersensitive ECL kit (Cat. #P0018S; Beyotime Biotechnology). Finally, the density values of the protein bands were captured and documented through a gel image analysis system (ChemiDoxTM, Bio-Rad, USA). GAPDH was used as the loading control.

2.7. Metabolomics

Metabolic profiling was executed using UHPLC-HRMS/MS instrumentation with dual-polarity electrospray ionization to ensure comprehensive coverage of diverse metabolite classes. Compound annotation integrated exact mass measurements, chromatographic alignment, and MS/MS spectral matching against validated HMDB and KEGG metabolite databases. Relative quantification employed batch-corrected peak intensity normalization with internal standard calibration.

2.8. Tissue NE concentration detection

A human NE enzyme-linked immunosorbent assay (ELISA) kit (Cat. #CSB-E07021h) and a mouse NE ELISA kit (Cat. #CSB-E07870m) were purchased from CUSABIO (Wuhan, China). NE levels in tumor tissues were determined by ELISAs according to the manufacturer's instructions.

2.9. Cell viability assessment

The cells were exposed to NE or quercetin at the indicated concentrations for 24, 48, or 72 h. Cell viability was evaluated *via* an MTT assay (Cat. #V13154; Gibco, NY, USA). An automated microplate spectrophotometer (BioTek Instruments, Winooski, VT, USA) was used to determine the absorbance of each well at 490 nm.

2.10. Colony formation assay

The cells were seeded in 6-well plates (200 cells/well in 2000 μL) and cultured for approximately 14 days. Colonies with more than 50 cells per colony were treated with vehicle or NE and quercetin-containing medium for 48 h. Subsequently, the medium was removed, and the cells were washed twice with PBS. After the cells were fixed with 4% paraformaldehyde, the colonies were stained with Giemsa for 5 min, and images were taken to record the results.

2.11. Wound healing

Cells were seeded in 6-well plates at 1×10^5 cells/well. Following 16-hour incubation, the complete medium was switched to fresh low-serum (2%) medium. Upon reaching 90% confluency, uniform linear wounds were generated in each well using a sterile 10-μL pipette tip. After rinsing twice with PBS to remove dislodged cells, cultures were maintained in serum-free medium. Reference markers were inscribed along the wound edges to standardize imaging regions. Wound closure dynamics were documented by inverted microscopy at baseline (0 h) and post-migration (48 h) time points.

2.12. Flow cytometric analysis

Apoptotic cell analysis was conducted *via* an Apoptosis and Necrosis Assay Kit (Cat. #C1056; Beyotime Biotechnology) and analyzed by a BD FACSCelesta flow cytometer (BD Biosciences, San Diego, CA). Cell survival after NE and/or quercetin intervention was measured by flow cytometry according to the manufacturer's instructions. In addition, flow cytometry was used to analyze the proportion of $CD8^+$ T cells in the tumor immune microenvironment and the proportion of interferon gamma (IFN-γ)-positive $CD8^+$ T cells.

2.13. EdU labeling assay

A total of 5×10^4 human BC SUM159PT, human BC MCF7, and mouse BC Py230 cells were treated with various concentrations of NE or/and quercetin. Following a 48-h incubation period, the BeyoClick™ EdU Cell Proliferation Kit (Cat. #C0071S, Beyotime Biotechnology) was used to quantify proliferating cells in *in vitro* cultures and tissue sections. Photomicrographs were captured immediately *via* an inverted microscope at 100 × magnification (Nikon, Japan).

2.14. Animal experiment and sample collection

In the Fig. 4, we present a schematic diagram of each part of the animal experiment. The mice in the chronic unpredictable mild stress (CUMS) group were subjected to CUMS, which included fasting, water fasting, tail clamping, restraint, diurnal reversal, tilting, wet bedding, and strobing, without the same stimuli on two consecutive days. After 4 weeks of CUMS, the mice were subcutaneously inoculated with Py230 BC cells (1×10^6 cells in 100 μL), and all the depression-modeling groups continued to receive CUMS. Quercetin (2.5 or 5 $mg \cdot kg^{-1}$, intraperitoneal injection once a day for 28 days) was administered to the mice in the quercetin-related group, and the same volume of saline was administered to the mice in the control group. The tumor volume was measured every 7 days, and the tumor size was calculated using the following equation: tumor volume = ½ (length × $width^2$). Twenty-eight days after treatment, the mice were anesthetized with pentobarbital (intraperitoneal injection, 100 $mg \cdot kg^{-1}$) and sacrificed by cervical dislocation. The tumor tissue was retained for subsequent experiments.

2.15. Behavioral assays

2.15.1. Open field test (OFT)

All experimental mice were individually housed in sanitized observation chambers (40 cm × 40 cm × 30 cm dimensions), where their spontaneous motor activity was continuously monitored using an infrared camera system. Each 5-minute trial was conducted under dim lighting conditions (50 lux) to minimize environmental stress. The EthoVision XT 3.0 behavioral analysis platform (Noldus Information Technology, Netherlands) was employed for video processing and statistical computation of locomotor metrics.

2.15.2. Forced swimming test (FST)

The behavioral assessment was performed in a standardized plexiglass cylinder (internal diameter 22 cm, height 25 cm) containing dechlorinated water maintained at 22–24 °C (depth 15 cm). A lateral-view digital tracking system (60 Hz sampling rate) continuously recorded whole-body displacement dynamics throughout the 300-second trial period. Quantitative analysis included two distinct behavioral states: passive floating (immobility threshold ≤ 1.25 cm/s), and active escape behaviors (struggle threshold > 6.25 cm/s), automatically quantified using threshold-based algorithms.

2.15.3. Sucrose preference test (SPT)

In this experiment, the animals were first accustomed to a 2% sucrose solution. After acclimatization, the mice were deprived of drinking water for 24 h. Two preweighed bottles (one

with 2% sucrose solution and one with tap water) were then provided for the mice to choose from over an 8-h period. The positions of the two bottles were swapped after 4 h of the experiment to avoid position preference. The weights of the bottles before and after the exchange were recorded, and the sucrose preference rate (%) was calculated using the following formula: sucrose preference rate (%) = [sucrose consumption/(sucrose consumption + tap water consumption)] × 100%.

2.16. Establishment and transfection of adenovirus

The adenoviral gene delivery system was implemented using Ad5 vectors to mediate PPARγ overexpression in murine Py230 mammary carcinoma cells. The adenoviral particles were generated through lipofectamine-mediated transfection in HEK-293A adenoviral packaging cells. Py230 cells were transfected at multiplicity of infection 50 for 48 h incubation periods prior to harvest for downstream functional assays.

2.17. Molecular docking

The binding affinity between quercetin and PPARγ was validated by molecular docking. The 3D structure of quercetin was obtained from the PubChem database. The PPARγ protein structures acquired from the RCSB PDB database (https://www.rcsb.org) served as receptors, and these structures were visualized separately using PyMOL and subjected to dehydration, hydrogenation, and charge calculations through Mgtools (version 1.5.6). Ligand and receptor structures were saved as pdbqt files. Subsequent molecular docking was performed utilizing AutoDock Vina (version 1.5.6), and the resulting higher-scoring conformations were visualized with PyMOL. The PLIP web tool (https://plip-tool.biotec.tu-dresden.de/plip-web/plip/index) facilitated the visualization of docking points.

2.18. Cellular thermal shift assay (CETSA)

The SUM159PT cells were lysed by being repeatedly frozen and thawed with liquid nitrogen 3 times. The cell lysates were divided into two aliquots, one as the control and the other treated with quercetin (100 μmol·L^{-1}) for 30 min at room temperature. Then, the lysates were heated at the desired temperatures (57–73 °C) and cooled on ice. The protein bands were detected with WB.

2.19. Terminal-deoxynucleotidyl transferase mediated nick end labeling (TUNEL) staining

Tumor specimens preserved in formalin fixation underwent paraffin embedding followed by sectioning into sequential 4-μm slices using microtomy. Post-embedding processing included xylene-mediated dewaxing prior to experimental staining. Apoptotic cells were visualized through standardized TUNEL assay implementation (Cat. #ATK00001, AtaGenix, Wuhan) with strict adherence to provider protocols. Subsequent nuclear counterstaining employed DAPI solution (0.05 μg·mL^{-1}, Cat. #G1012, Servicebio, Wuhan) with 10 min incubation, preceded by triple PBS washing cycles to remove residual reagents. Mounted sections were subjected to fluorescence microscopy analysis (NIKON Eclipse ci, Japan) at 400 × optical magnification for cellular-level observation.

2.20. Statistical analysis

Quantitative results are expressed as mean ± SD throughout this study. Statistical analyses were performed using SPSS 13.0 (IBM, USA) with complementary data visualization accomplished through GraphPad Prism 9 (GraphPad Software, USA). Intergroup comparisons employed one-way ANOVA while longitudinal measurements utilized repeated-measures ANOVA methodology. The statistical significance threshold was established at α = 0.05 for all experimental outcomes.

3. Results

3.1. MR shows that depression is a risk factor for BC

The results of the MR analysis are presented in Fig. 1, including a schematic diagram of the research design (Fig. 1A), a forest plot (Fig. 1B), a scatter plot (Fig. 1C), a funnel plot (Fig. 1D), and a leave-one-out analysis plot (Fig. 1E). In this study, the correlation between depression as an exposure and BC as an outcome was analyzed by using MR analysis. The results between depression and BC were statistically significant: P = 0.006 and 95% CI = 1.011–1.067. The leave-one-out analysis also did not reveal any abnormal single nucleotide polymorphisms (SNPs). The results of reverse MR analysis are presented in Fig. 1F. Considering cross-validation, we did not find any reverse causal relationships between BC and depression (P = 0.066, 95% CI = 0.831–1.006).

3.2. PPARγ expression was inhibited in the tumor tissues of depressed BC patients

Next, we divided the BC patients into nondepressed and depressed groups on the basis of the HAMD-17 scale and HAMA scale (Figs. 2A, 2B). Transcriptomic analysis of tumor tissues revealed significant differences in the expression profiles between the nondepression and depression groups (Figs. 2C, 2D, and 2E). Compared with the nondepression group, the depression group had 556 genes with increased expression and 1100 genes with decreased expression. KEGG pathway enrichment analysis of the DEGs revealed that the PPAR signaling pathway was significantly enriched (Fig. 2F). Gene set enrichment analysis (GSEA) of the PPAR signaling pathway revealed that PPARG expression was inhibited in the depression group (Fig. 2G).

Given that the PPAR gene family consists of PPARα, PPARβ, and PPARγ, we analyzed the relationship between the expression of these three genes in tumors and patient prognosis (Figs. 2H, 2I, and 2J). We found that low PPARG expression is a risk factor for prognosis in patients with BC. Using IF and WB to validate the tumor tissues of patients in the nondepression and depression groups, we determined that PPARγ protein expression in the BC tissues of patients in the depressed group was significantly reduced (Figs. 2K, 2L).

3.3. NE inhibited PPARγ expression and promoted the proliferation of BC cells

Furthermore, we performed metabolomic analysis of BC tissues collected from patients. The results revealed significant differences in tumor tissue metabolites between the nondepression and depression groups, with 62 metabolites increasing and 10 metabolites decreasing (Figs. 3A, 3B, 3C and 3D). The level of NE in the tumor tissue of the depression group was significantly greater than that in the nondepression group (Figs. 3D and 3E).

Therefore, we used NE to treat human BC cells and found that 10 μmol·L^{-1} NE significantly promoted the viability of BC cells (Figs. 3). The results of the colony formation and wound healing assays revealed that NE promoted the clonal proliferation and migration of BC cells (Figs. 3). Flow cytometry revealed that NE inhibited the apoptosis of BC cells and promoted their survival (Fig. 3J). EdU cell proliferation experiments revealed that NE promoted the proliferation of BC cells (Fig. 3K). This evidence suggests that abnormally elevated NE levels in BC tissues may promote tumor cell growth in depressed states and have a con-

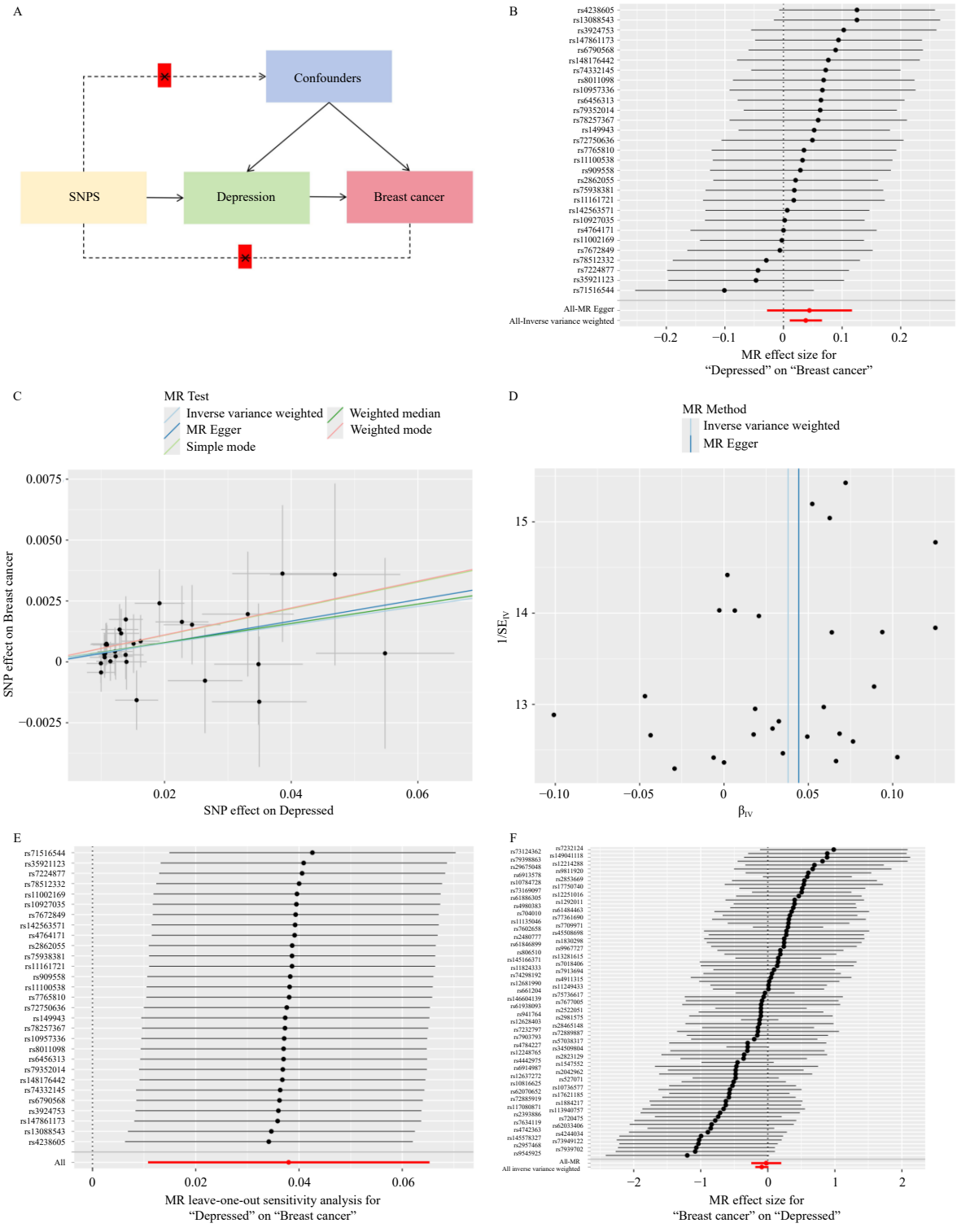


Fig. 1 Two-sample MR analysis of depression and BC patients. (A) Diagram of the study design for MR. (B) Forest plot for the causal SNP effect of depression on BC incidence. The error bars indicate the 95% confidence intervals (CIs). (C) Scatter plot of the causal SNP effect of depression on BC incidence. We plot each black point to represent each SNP on the exposure (horizontal axis) and the outcome (vertical axis), with error bars corresponding to each standard error (SE). The slope of each line corresponds to the combined estimate *via* the inverse variance weighted (light blue line), MR–Egger (blue line), simple (light green line), weighted median (green line), and weighted (pink line) methods. (D) Funnel plot for the causal SNP effect of depression on BC incidence. (E) Leave-one-out analysis plot for the causal SNP effect of depression on BC. The error bars indicate the 95% CI. (F) Forest plot of the causal SNP effect of BC on depression.

centration effect.

3.4. Chronic stress promoted tumor growth in mice, which was accompanied by the inhibition of PPARγ expression and increased NE infiltration

The experimental process for generating chronic stress-induced BC model mice *in vivo* is shown in Fig. 4A. After 28 days of CUMS, the mice presented obvious depression, indicating that we successfully established a depression mouse model (Figs. 4B, 4C, and 4D). Compared with that in the NC group, tumor growth was significantly accelerated in the CUMS group (Figs. 4E, 4F, and 4G). The level of NE in the tumor tissue of the CUMS group was significantly greater than that in the NC group (Fig. 4H). The tumor tis-

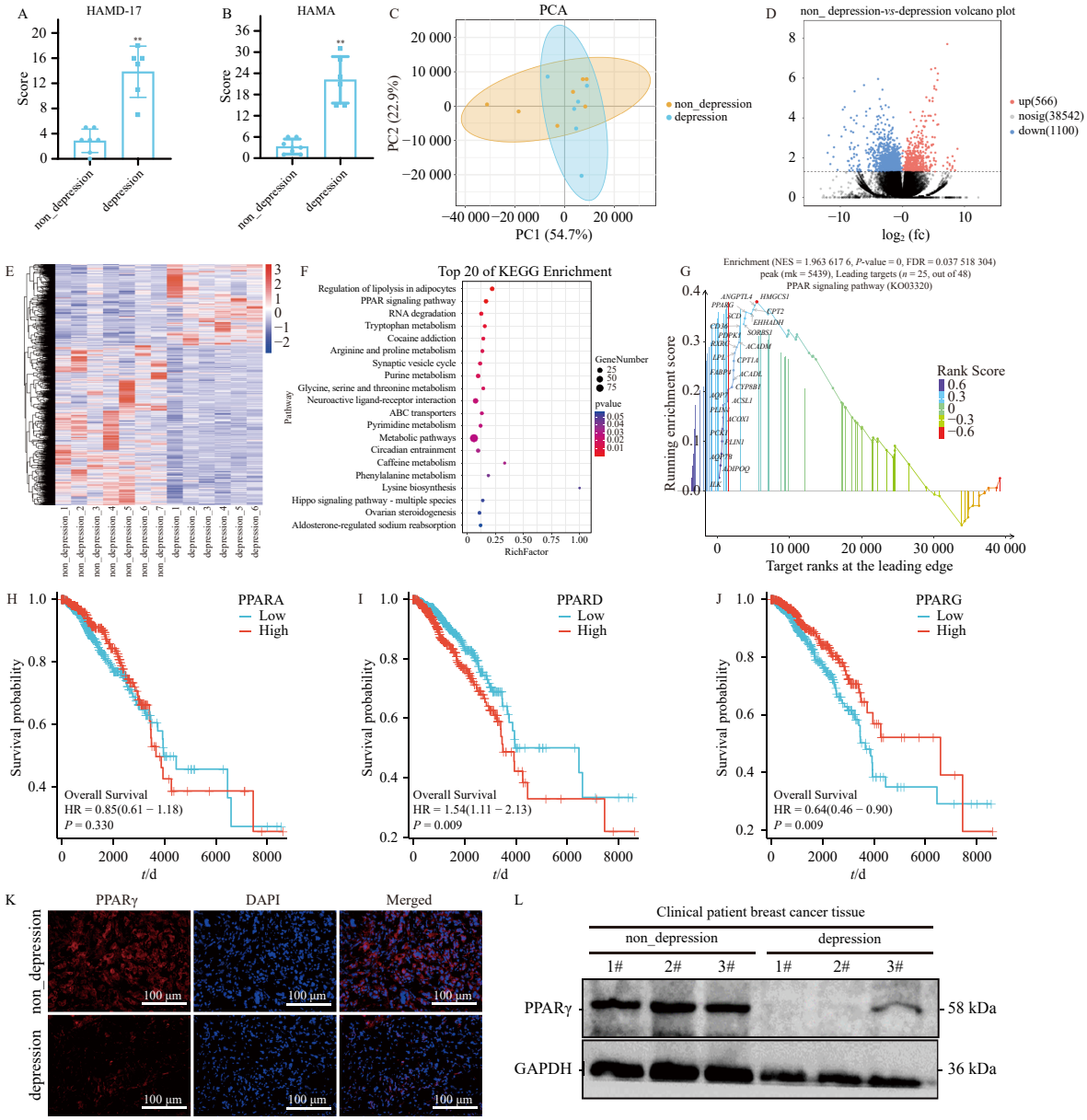


Fig. 2 Transcriptomic analysis and validation of tumor tissue in patients with BC. (A) BC patient HAMD-17 scale score. (B) BC patient HAMA scale score. (C) Principal component analysis (PCA) map. (D) Volcano map. (E) Heatmap. (F) KEGG pathway enrichment of DEGs between the nondepression group and the depression group. (G) GSEA of the nondepression group and depression group. (H), (I), and (J) Kaplan–Meier curves of PPAR gene expression in BC. (K) IF staining of tumor tissue from BC patients. (L) WB of tumor tissue from BC patients. The data are presented as the means ± SDs; $^{**}P < 0.01$ *vs* the nondepression group; nondepression group, $n = 7$; depression group, $n = 6$.

sues of these two groups were verified by IF and WB, and we determined that the protein expression of PPARγ in the BC tissues of the CUMS group mice was significantly decreased (Figs. 4I, 4J).

3.5. PPARγ regulated tumor growth and was targeted by quercetin

We constructed a Py230 cell line overexpressing PPARγ (Fig. 5A). The results of the MTT experiment revealed that overexpression of PPARγ reversed the inhibitory effect of NE on the viability of BC cells (Fig. 5B). The results of the colony formation and EdU cell proliferation experiments revealed that the overexpression of PPARγ inhibited the NE-mediated colony formation and proliferation of BC cells (Fig. 5C, 5D). *In vivo* experiments also revealed that overexpression of PPARγ in BC cells significantly inhibited the tumor-promoting effect of CUMS (Figs. 5E, 5F, 5G, and 5H). The results of molecular docking indicate that quercetin has good binding potential with the active pocket of the PPARγ protein (Fig. 5I). To validate the interactions between quercetin and PPARγ in cells, we performed a CETSA. The results revealed that quercetin treatment effectively protected PPARγ protein from temperature-dependent degeneration, suggesting that quercetin can directly target PPARγ (Fig. 5J). Next, through IF and WB, we confirmed that NE can inhibit PPARγ expression in BC cells and that this inhibitory effect can be reversed by quercetin (Figs. 5K, 5L).

3.6. Quercetin regulated the PPARγ signaling pathway to interfere with the BC-promoting effect of NE and chronic stress

The results of the MTT assay revealed that 100 μmol·L^{-1} quercetin reversed the increased activity of the BC cells induced by NE (Figs. 6A, 6B, and 6C). Clonal formation and EdU cell proliferation experiments revealed that quercetin inhibited the acceleration of Py230 cell proliferation mediated by NE (Figs. 6D, 6G). Wound healing and WB results revealed that quercetin inhibited the Py230 cell migration enhancement and epithelial–mesenchymal transition (EMT) changes mediated by NE (Figs. 6E, 6H). Flow cytometry and WB results revealed that quercetin reversed

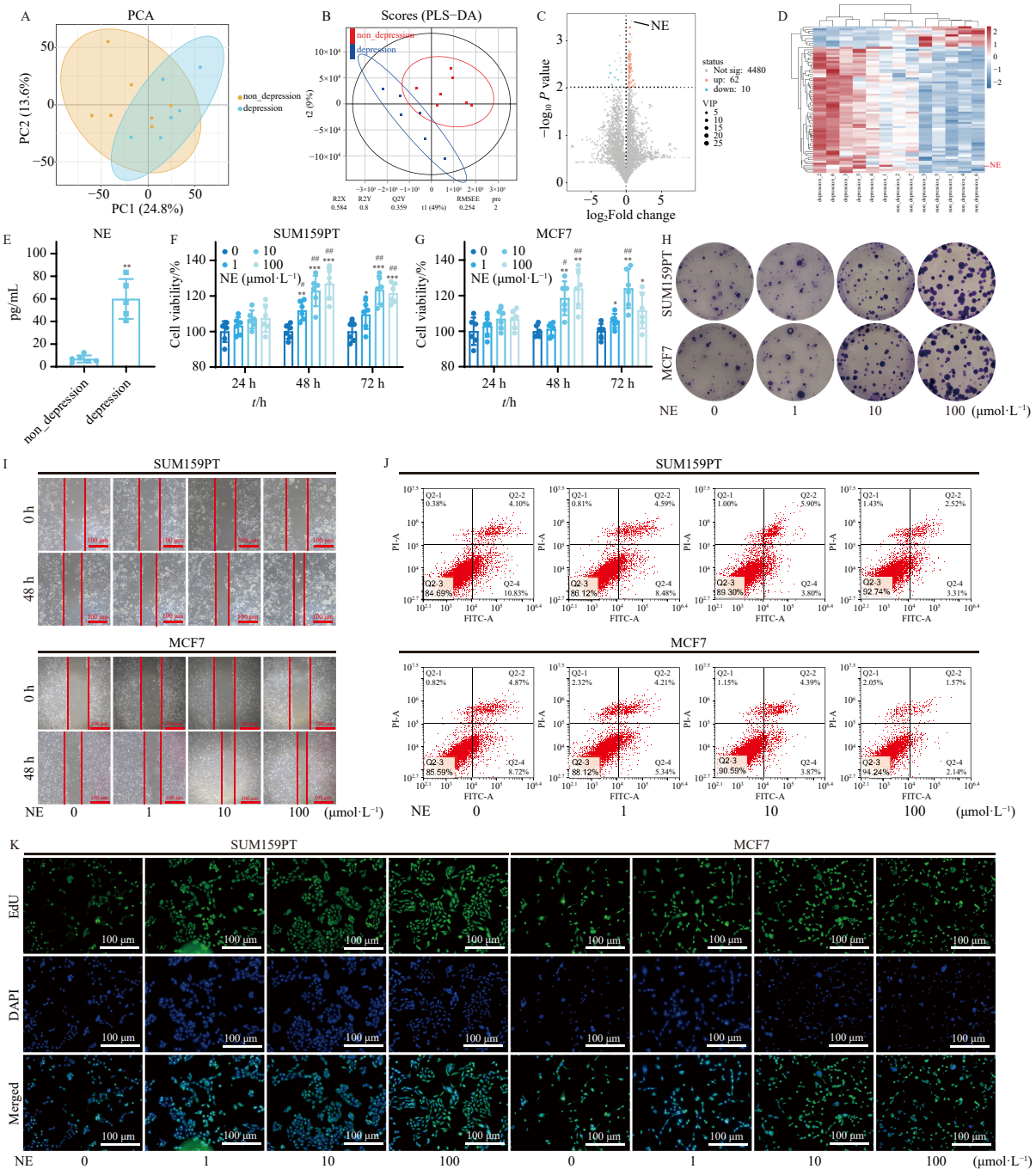


Fig. 3 Metabolomic analysis and validation of tumor tissue in patients with BC. (A) PCA map. (B) Partial least squares discrimination analysis (PLS-DA) map. (C) Volcano map. (D) Heatmap. (E) The concentration of NE was determined by ELISAs. (F), (G) Cell viability of SUM159PT and MCF7 cells treated with different concentrations of NE in medium for 24, 48, and 72 h. (H) Giemsa-stained colonies were observed under an inverted microscope. (I) Wound healing was observed under an inverted microscope. (J) Flow cytometric analysis of apoptotic cells. (K) EdU-labeled cell proliferation experiments. (A)–(E) $^{**}P < 0.01$ *vs* the nondepression group; nondepression group, $n = 7$; depression group, $n = 6$. (F)–(K) $^{*}P < 0.05$, $^{**}P < 0.01$, $^{***}P < 0.001$ *vs* the 0 μmol·L^{-1} NE group; $^{\#}P < 0.05$, $^{\#\#}P < 0.01$ *vs* the 24 h group; $n = 6$.

the NE-mediated spontaneous inhibition of Py230 cell apoptosis (Figs. 6F, 6H).

The in vivo results revealed that quercetin can inhibit the progression of BC in a CUMS mouse model in a dose-dependent manner. However, there was no significant effect on tumor progression in mouse BC models with normal mood (Figs. 6I, 6J, 6K, and 6L). Further verification revealed that quercetin could reverse CUMS-mediated antiapoptotic effects and EMT changes in BC (Figs. 6M, 6N).

3.7. Quercetin reshaped the tumor immune microenvironment in chronically stressed mice

With the BC data in the TCGA database, we used the ESTIMATE algorithm to analyze the significance of PPARγ expression in BC. We found that the expression level of PPARγ was positively correlated with the tumor immune score (Fig. 7A). Therefore, we used this algorithm to analyze transcriptomic data from the BC tissues of our clinical patients. The results revealed that even when one sample from the nondepression group had an abnormal score, the immune score of the depression group still decreased by 14.03% (Fig. 7B). We further used the single sample GSEA (ssGSEA) algorithm to analyze the relationship between the expression of PPARγ and the type of cells that are immunologically infiltrated into the BC microenvironment. We found that among the major antitumor immune cell subtypes, $CD8^+$ T cells were the immune cells with the strongest correlation with PPARγ expression (Fig. 7C). To verify these results, we used flow cyto-

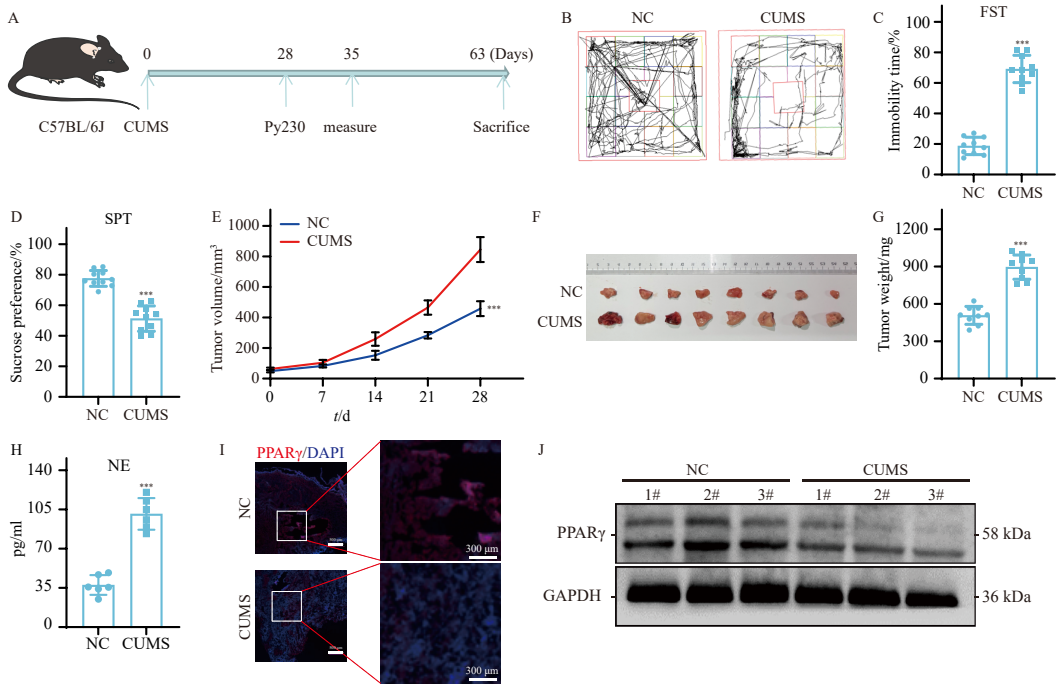


Fig. 4 Effects of CUMS on BC. (A) Schematic diagrams of the experiments. (B) OFT track map. (C) Percentage of total immobility time during the FST. (D) Sucrose preference rate. (E) Tumor size was measured every 7 days. (F) Representative images of Py230 tumor tissues. (G) Tumor tissue weight after 28 days. (H) NE concentrations in tumor tissue. (I) IF staining of tumor tissue. (J) WB of tumor tissue. The data are presented as the means ± SDs; $^{***}P < 0.001$ *vs* the NC group; $n = 10$ or $n = 6$.

metry to analyze $CD8^+$ T-cell infiltration in BC tissues from different groups of immunologically normal mice. The results revealed that the proportion of $CD8^+$ T cells in the BC tissues of the CUMS group was significantly decreased, and the proportion of cytotoxic $CD8^+$ T cells (IFN-γ positive) was also significantly decreased. After quercetin treatment, these antitumor immunosuppressive effects were partially reversed (Fig. 7D).

We used T-cell-deficient nude mice to verify whether $CD8^+$ T cells participate in the tumor-promoting effects of depression and the anticancer effects of quercetin in depressed states (Fig. 7E). Compared with that in the normal immune model mice, the tumor-promoting effect of depression was significantly reduced in the T-cell-deficient nude mice (97.1% *vs* 25.0%). Quercetin also inhibited depression-mediated tumor-promoting effects in the nude mice, but the effect was significantly weaker than that in the normal immune model mice (43.6% *vs* 15.7%) (Figs. 7F and 7I).

4. Discussion

The unclear mechanism by which depression promotes the progression of BC has led to the insufficiency of current BC treatments, thus strengthening the global scientific pursuit of the key molecular mechanisms by which depression promotes cancer. As an effective technology for discovering key molecular targets, high-throughput sequencing has been widely used in bioscience research. However, owing to the inconvenience of collecting clinical samples, no transcriptomic or metabolomic data on cancer tissues from depressed BC patients have been published.

In this study, on the basis of transcriptomic data from clinical samples of BC patients, we demonstrate for the first time that PPARγ expression is suppressed in the BC tissues of depressed patients. Previous studies reported that low expression of PPARγ is associated with poor prognosis in patients with tumors [20]. In addition, low expression of PPARγ may promote tumor proliferation and migration [21]. During the malignant progression of a tumor, tumor cells secrete cytokines, exosomes and other signaling molecules [22] that interfere with the migration of immune cells into the tumor or inhibit the ability of immune cells to kill the tumor [23, 24], forming an inhibitory tumor immune microenvironment and ultimately promoting the process of cancer. Previous studies have confirmed that PPARγ can degrade PD-L1 by activating autophagy, thereby inhibiting the expression of PD-L1 on tumor cells [25], and that PD-L1 can bind to PD-1 on $CD8^+$ T cells, inhibit the activation of $CD8^+$ T cells [24, 26], and even lead to programmed death of $CD8^+$ T cells [27], resulting in tumor immune evasion, which is also a key target of tumor immunotherapy. Our results show that PPARγ promotes the spontaneous apoptosis of tumor cells and inhibits their proliferation and migration. In addition, our results revealed that the tumor-promoting effect of chronic stress was more significant in immunonormal mice than in T-cell-deficient mice, which may be related to the reduction in infiltration and inactivation of $CD8^+$ T cells, suggesting that depression promotes immune desertification in the tumor microenvironment. However, whether this finding is related to the effect mediated by the inhibition of PPARγ expression in tumor cells needs to be further verified.

Similarly, through the use of metabolomics based on clinical BC samples, we identified significantly elevated concentrations of NE in tumor tissues from depressed patients. NE is a stress hormone released by the body in response to external stimuli and chronic stress [28]. Pharmacological studies have shown that duloxetine, an NE reuptake inhibitor, can increase the protein expression of PPARγ in the prefrontal cortex and hippocampus of depressed animal models and reverse the depression-induced transcriptional inhibition of PPARγ [29]. Other studies have confirmed that NE can also inhibit the expression of PPARγ, promote cell proliferation and inhibit cell differentiation [30, 31]. Unfortunately, the effect of this NE mediated by PPARγ on tumor cells has not been reported. Therefore, we further verified this result (Figs. S1A, S1B). However, *in vitro* results revealed that NE had no significant effect on the viability or migration of $CD8^+$ T cells [32]. In ovarian cancer, the NE receptor antagonist propranolol was shown to increase the activity of $CD8^+$ T cells in a coculture system by inhibiting the release of extracellular vesicles by tumor cells. Animal experiments have shown that reducing chronic behavioral stress increases tumor metastasis [33]. These findings further suggest that NE does not directly act on $CD8^+$ T cells but may indirectly affect $CD8^+$ T cells through the intermediary effect of tumor cells, ultimately leading to changes in the immune microenvironment (Fig. S1C).

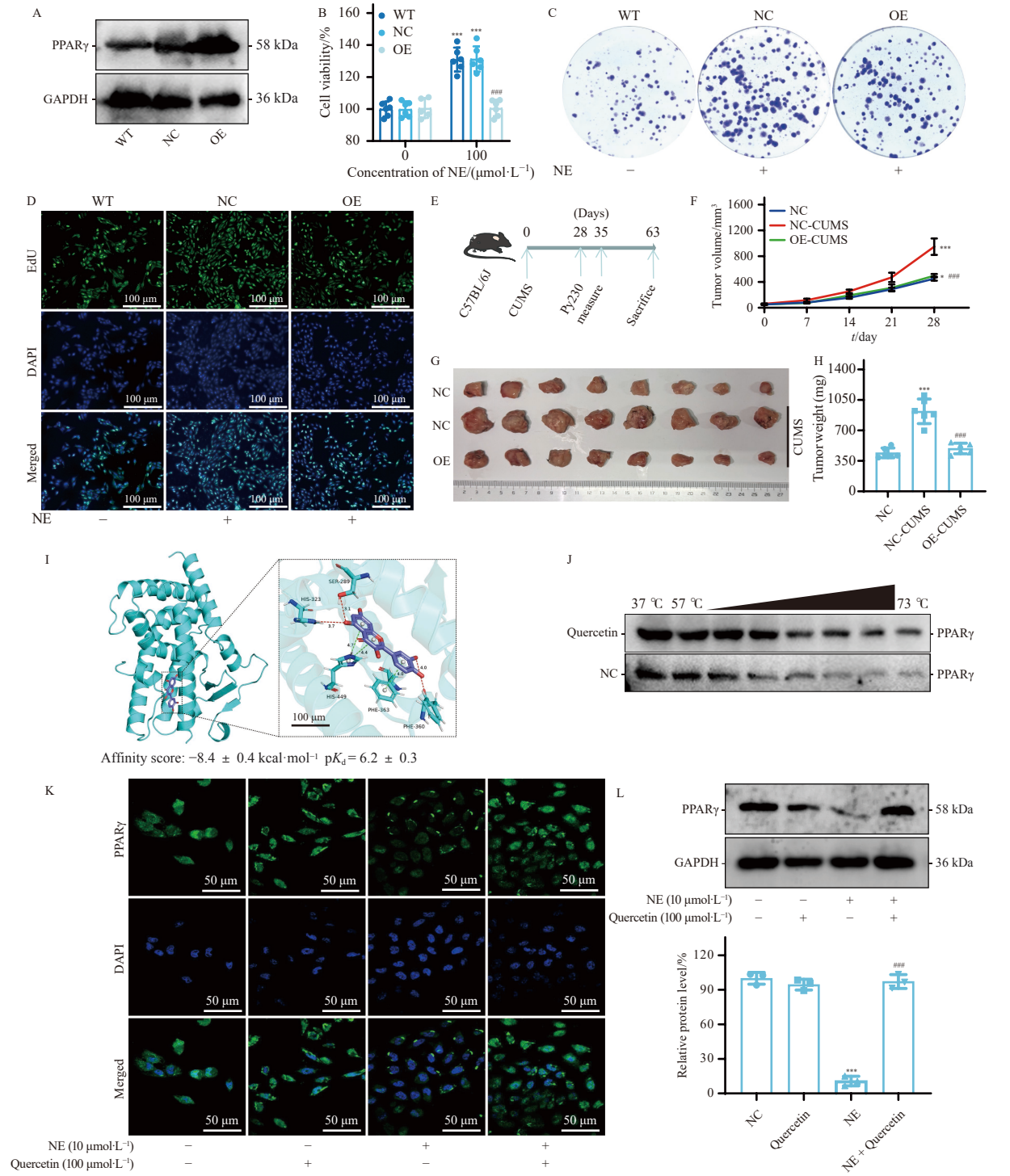


Fig. 5 Effect of PPARγ on tumors and intervention with quercetin. (A) WB verification of PPARγ protein overexpression in Py230 cells. (B) Viability of Py230 cells overexpressing PPARγ treated with different concentrations of NE in the medium for 48 h. (C) Giemsa-stained colonies were observed under an inverted microscope. (D) EdU-labeled cell proliferation experiments. (E), (F), (G), and (H) Effects of a depressed mouse model on tumor growth in Py230 cells overexpressing PPARγ. (I) Molecular docking results of the quercetin and PPARγ proteins. (J) CETSA results. (K), (L) Effects of NE and/or quercetin on PPARγ protein expression in SUM159 cells. The data are presented as the means ± SDs; $^{***}P < 0.001$ *vs* the WT/NC group; $^{\#\#\#}P < 0.001$ *vs* the NC/NC-CUMS/NE group; $n = 10$ or $n = 3$.

Natural products, which are esteemed for their rich legacy in offering essential molecular frameworks for drug discovery, have attracted increased interest for their potential in cancer treatment [34-36]. To date, several widely applied anticancer drugs in the clinic are derived from natural products, including irinotecan, vincristine, etoposide, and paclitaxel. Quercetin is derived from a variety of common plant foods and Chinese herbs, of which black tea has been shown to treat depression-related dementia [37] and onion has been shown to treat depression-related hypomnesia [38] and irritable bowel syndrome [39], and traditional Chinese medicine formulas rich in quercetin can help alleviate depression-related muscle damage [40-42]. Although there has been no in-depth analysis of the active ingredients involved in these studies, we can infer from the common characteristics of these food or natural products that quercetin may play an important role. Given the vast range of pharmacological activities of quercetin, our research is valuable for elucidating the anticancer potential of quercetin, promoting the development of quercetin-based therapeutic strategies. We demonstrated for the first time that quercetin can target PPARγ and regulate the abnormal proliferation of can-

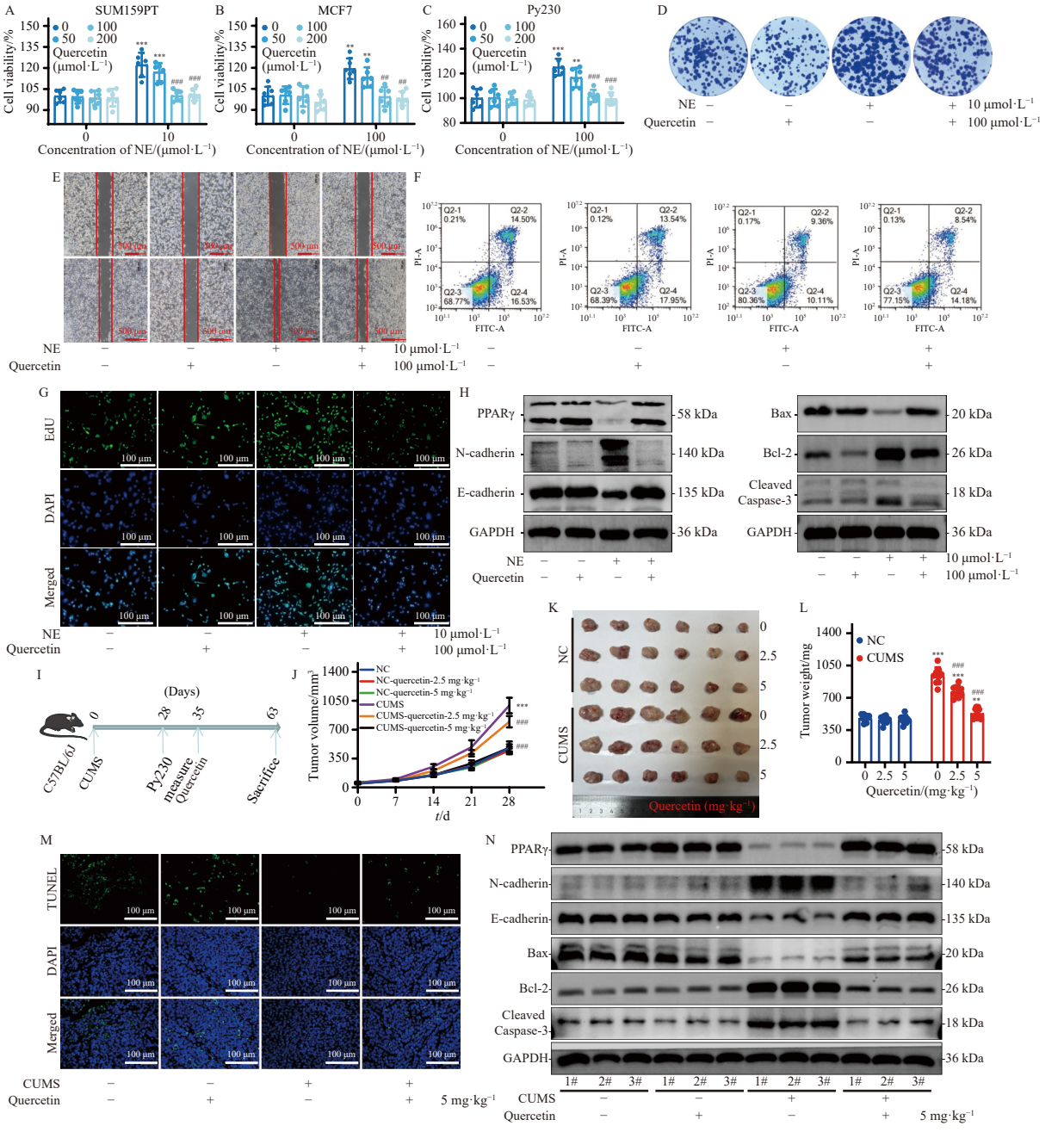


Fig. 6 Effects of quercetin on BC. (A), (B), and (C) Cell viability of SUM159PT, MCF7, and Py230 cells treated with different concentrations of NE and/or quercetin in medium for 48 h. (D) Giemsa-stained colonies were observed under an inverted microscope. (E) Wound healing was observed under an inverted microscope. (F) Flow cytometric analysis of apoptotic cells. (G) EdU-labeled cell proliferation experiments. (H) Protein expression in cell cultures. (I), (J), (K), and (L) Antitumor effects of quercetin *in vivo*. (M) TUNEL staining of tumor samples. (N) WB analysis was performed to analyze the expression levels of EMT- and apoptosis-related proteins in tumor tissues. The data are presented as the means ± SDs; $^{**}P < 0.01$, $^{***}P < 0.001$ *vs* the 0 μmol·L^{-1} NE/NC group; $^{\#\#\#}P < 0.001$ *vs* the 100 μmol·L^{-1} NE/CUMS group; $n = 10$ or $n = 6$.

cer cells with low PPARγ expression and demonstrated that quercetin has no significant effect on cancer cells with normal PPARγ expression. In addition, we found that quercetin had no significant effect on CD8$^+$ T infiltration in the tumor microenvironment in nondepressed states, suggesting that the regulation of quercetin is highly targeted, which may be an important factor in the low toxicity of quercetin.

Importantly, in this study, we identified the key metabolite NE and the key gene PPARγ for the cancer-promoting effect of depression, which has never been reported in previous studies, and our work can provide a reference for further research on depression-related tumors. In addition, we found that quercetin from a variety of food and herbal sources can target PPARγ, which provides a very good example for treating depression-related malignancies and other diseases in daily life, and we can attempt more lifestyle changes, such as diet modifications, to alleviate the disease rather than choosing more drugs with side effects. Finally, maintaining positive emotions is the simplest and most practical way to curb BC progression in daily life.

5. Conclusions

In summary, on the basis of clinical patient-sourced data, we identify for the first time that PPARγ is a key factor in the promotion of BC progression by depression, and in addition, we provide evidence that depression may inhibit PPARγ expression through NE. Moreover, PPARγ may participate in the tumor-promoting effect of depression by influencing the infiltration of CD8$^+$ T cells in the tumor immune microenvironment. Finally, we confirmed that quercetin can target PPARγ and interfere with the tumor-promot-

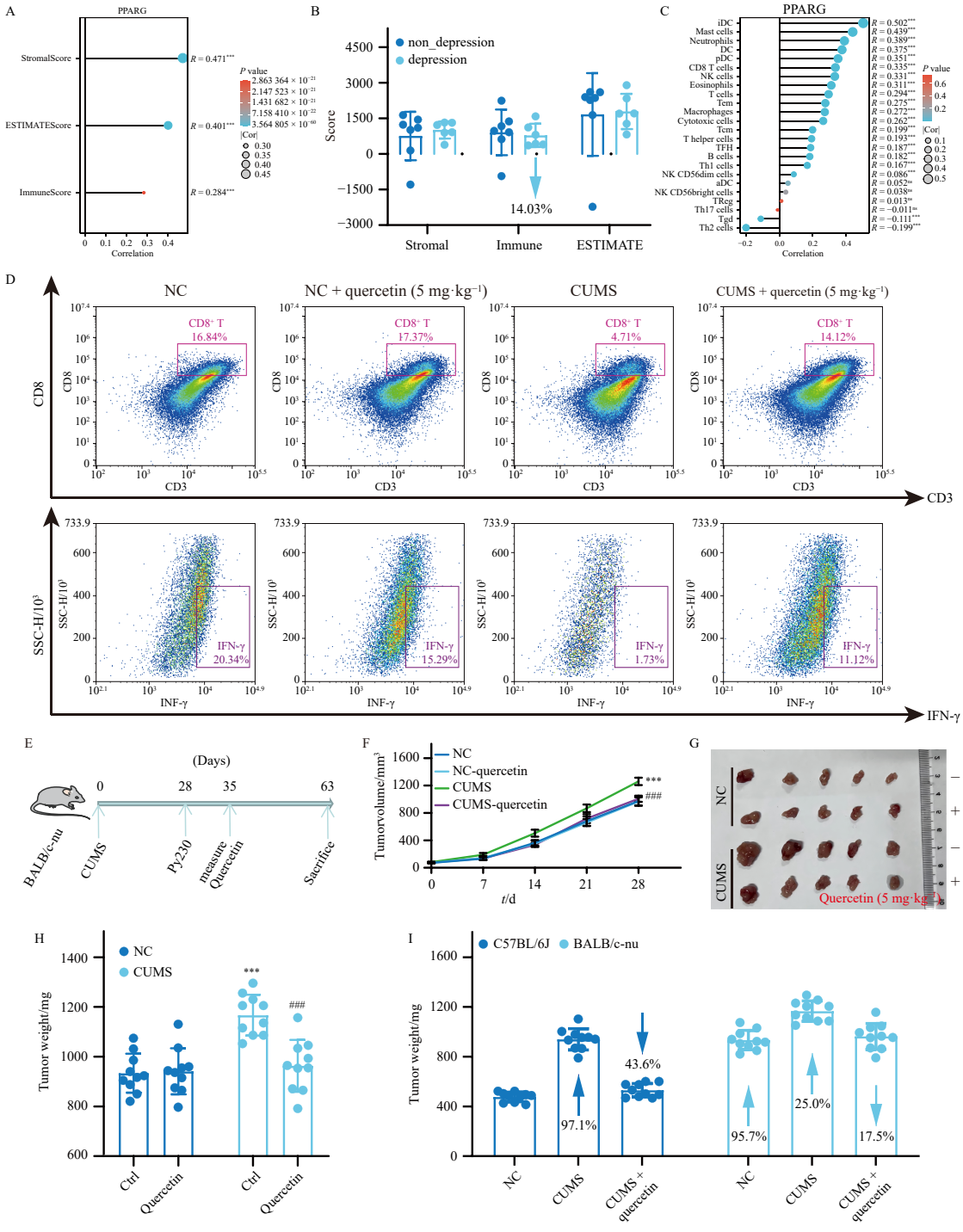


Fig. 7 Effect of quercetin on the immune microenvironment of BC tumors. (A) Effect of the PPARγ expression level on the immune infiltration score. (B) Effect of depression on the immune infiltration score. (C) Relationships between the expression level of PPARγ and the infiltration subtypes of immune cells in the tumor microenvironment. (D) Immunoinfiltration of tumor tissue was analyzed by flow cytometry. (E), (F), (G), and (H) Antitumor effects of quercetin on nude mice with T-cell deficiency. (I) Comparison of the effects of depression on tumor promotion and quercetin intervention in mice with different immune states. The data are presented as the means ± SDs; $^{***}P < 0.001$ *vs* the NC group; nondepression group, $n = 7$; depression group, $n = 6$.

ing effects of depression.

Funding

This work was supported by the National Natural Science Foundation of China (Nos. 82274513, 82305234 and 82474504), the Guangdong Basic and Applied Basic Research Foundation (No. 2023A1515011115), the Incubation Program for the Science and Technology Development of Chinese Medicine Guangdong Laboratory (No. HQL2024PZ023), the Planned Science Technology Project of Guangzhou (Nos. SL2023A03J01120, SL2023A04J00228, and 2024A03J0850), the Project of Guangdong Provincial Key Laboratory of Clinical Research on Traditional Chinese Medicine Syndrome (No. YN2023ZH10), the Autonomous Project of State Key Laboratory of Traditional Chinese Medicine Syndrome (No. QZ2023ZZ13), the Beijing Medical Foundation (No. MDK2023-1007), and the Science and Technology Innovation Medical Development Foundation of Beijing (No. KC2023-JX-0082-12).

Supporting Information

The datasets used and/or analyzed during the current study are available from the corresponding author upon reasonable re-

quest.

Declaration of competing interest

The authors declare that there are no conflicts of interest regarding the publication of this paper.

References

1 Siegel RL, Giaquinto AN, Jemal A. Cancer statistics, 2024. *CA Cancer J Clin*. 2024;74:12-49. https://doi.org/10.3322/caac.21820.
2 Sun YS, Zhao Z, Yang ZN, et al. Risk factors and preventions of breast cancer. *Int J Biol Sci*. 2017;13:1387-1397. https://doi.org/10.7150/ijbs.21635.
3 MacMahon B. Epidemiology and the causes of breast cancer. *Int J Cancer*. 2006;118:2373-2378. https://doi.org/10.1002/ijc.21404.
4 Battat M, Omair N, Wildali MA, et al. Assessment of depression symptoms among cancer patients: a cross-sectional study from a developing country. *Sci Rep*. 2024;14:11934. https://doi.org/10.1038/s41598-024-62935-x.
5 Sanjida S, Janda M, Kissane D, et al. A systematic review and meta-analysis of prescribing practices of antidepressants in cancer patients. *Psychooncology*. 2016;25:1002-1016. https://doi.org/10.1002/pon.4048.
6 Zhao L, Li X, Zhang Z, et al. Prevalence, correlates and recognition of depression in Chinese inpatients with cancer. *Gen Hosp Psychiatry*. 2014;36:477-482. https://doi.org/10.1016/j.genhosppsych.2014.05.005.
7 Wang YH, Li JQ, Shi JF, et al. Depression and anxiety in relation to cancer incidence and mortality: a systematic review and meta-analysis of cohort studies. *Mol Psychiatry*. 2020;25:1487-1499. https://doi.org/10.1038/s41380-019-0595-x.
8 Chen X, Kong J, Diao X, et al. Depression and prostate cancer risk: a Mendelian randomization study. *Cancer Med*. 2020;9:9160-9167. https://doi.org/10.1002/cam4.3493.
9 Massetti GM, Thomas CC, King J, et al. Mental health problems and cancer risk factors among young adults. *Am J Prev Med*. 2017;53:S30-S39. https://doi.org/10.1016/j.amepre.2017.04.023.
10 Wang X, Wang N, Zhong L, et al. Prognostic value of depression and anxiety on breast cancer recurrence and mortality: a systematic review and meta-analysis of 282,203 patients. *Mol Psychiatry*. 2020;25:3186-3197. https://doi.org/10.1038/s41380-020-00865-6.
11 Shin KJ, Lee YJ, Yang YR, et al. Molecular mechanisms underlying psychological stress and cancer. *Curr Pharm Des*. 2016;22:2389-2402. https://doi.org/10.2174/1381612822666160226144025.
12 Geng Q, Li L, Shen Z, et al. Norepinephrine inhibits CD8(+) T-cell infiltration and function, inducing anti-PD-1 mAb resistance in lung adenocarcinoma. *Br J Cancer*. 2023;128:1223-1235. https://doi.org/10.1038/s41416-022-02132-7.
13 Wang A, Wan X, Zhuang P, et al. High fried food consumption impacts anxiety and depression due to lipid metabolism disturbance and neuroinflammation. *Proc Natl Acad Sci U S A*. 2023;120:e2073870176. https://doi.org/10.1073/pnas.2221097120.
14 Luo T, Zhang Y, Liu X, et al. The central nervous system can directly regulate breast cancer progression and blockage by quercetin. *Ann Transl Med*. 2021;9:999. https://doi.org/10.21037/atm-21-2558.
15 Luo T, Liang Y, Chen L, et al. Effect of quercetin on the progression of breast cancer in mice with chronic stress by regulating the polarization of microglia. *J Funct Foods*. 2024;119:106294. https://doi.org/10.1016/j.jff.2024.106294.
16 Dabeek WM, Marra MV. Dietary quercetin and kaempferol: bioavailability and potential cardiovascular-related bioactivity in humans. *Nutrients*. 2019;11(10):2288. https://doi.org/10.3390/nu11102288.
17 Shorobi FM, Nisa FY, Saha S, et al. Quercetin: a functional food-flavonoid incredibly attenuates emerging and re-emerging viral infections through immunomodulatory actions. *Molecules*. 2023;28(3):938. https://doi.org/10.3390/molecules28030938.
18 Hartwig FP, Davies NM, Hemani G, et al. Two-sample Mendelian randomization: avoiding the downsides of a powerful, widely applicable but potentially fallible technique. *Int J Epidemiol*. 2016;45:1717-1726. https://doi.org/10.1093/ije/dyx028.
19 Mu H, Chen J, Huang W, et al. OmicShare Tools: a zero-code interactive online platform for biological data analysis and visualization. *iMeta*. 2024;3:e228. https://doi.org/10.1002/imt2.228.
20 Zhang Q, Xiong L, Wei T, et al. Hypoxia-responsive PPARGC1A/BAMBI/ACSL5 axis promotes progression and resistance to lenvatinib in hepatocellular carcinoma. *Oncogene*. 2023;42:1509-1523. https://doi.org/10.1038/s41388-023-02665-y.
21 Vallee A, Lecarpentier Y. Crosstalk between peroxisome proliferator-activated receptor gamma and the canonical Wnt/β-catenin pathway in chronic inflammation and oxidative stress during carcinogenesis. *Front Immunol*. 2018;9:745. https://doi.org/10.3389/fimmu.2018.00745.
22 Zhang L, Yu D. Exosomes in cancer development, metastasis, and immunity. *Biochim Biophys Acta Rev Cancer*. 2019;1871:455-468. https://doi.org/10.1016/j.bbcan.2019.04.004.
23 Naseri M, Bozorgmehr M, Zoller M, et al. Tumor-derived exosomes: the next generation of promising cell-free vaccines in cancer immunotherapy. *OncoImmunology*. 2020;9:1779991. https://doi.org/10.1080/2162402X.2020.1779991.
24 Lu Y, Zheng J, Lin P, et al. Tumor microenvironment-derived exosomes: a double-edged sword for advanced T cell-based immunotherapy. *ACS Nano*. 2024;18:27230-27260. https://doi.org/10.1021/acsnano.4c09190.
25 Gou Q, Che S, Chen M, et al. PPARγ inhibited tumor immune escape by inducing PD-L1 autophagic degradation. *Cancer Sci*. 2023;114:2871-2881. https://doi.org/10.1111/cas.15818.
26 Fang W, Zhou T, Shi H, et al. Progranulin induces immune escape in breast cancer *via* up-regulating PD-L1 expression on tumor-associated macrophages (TAMs) and promoting CD8(+) T cell exclusion. *J Exp Clin Cancer Res*. 2021;40:4. https://doi.org/10.1186/s13046-020-01786-6.
27 Kaltenmeier C, Yazdani HO, Morder K, et al. Neutrophil extracellular traps promote T cell exhaustion in the tumor microenvironment. *Front Immunol*. 2021;12:785222. https://doi.org/10.3389/fimmu.2021.785222.
28 Babic NL, Johnstone CP, Reljic S, et al. Evaluation of physiological stress in free-ranging bears: current knowledge and future directions. *Biol Rev Camb Philos Soc*. 2023;98:168-190. https://doi.org/10.1111/brv.12902.
29 Dionisie V, Filip GA, Manea MC, et al. The anti-inflammatory role of SSRI and SNRI in the treatment of depression: a review of human and rodent research studies. *Inflammopharmacology*. 2021;29:75-90. https://doi.org/10.1007/s10787-020-00777-5.
30 Bargut TC, Aguila MB, Mandarim-de-Lacerda CA. Brown adipose tissue: updates in cellular and molecular biology. *Tissue Cell*. 2016;48:452-460. https://doi.org/10.1016/j.tice.2016.08.001.
31 Zhou J, Liu Z, Zhang L, et al. Activation of β2-adrenergic receptor promotes growth and angiogenesis in breast cancer by down-regulating PPARγ. *Cancer Res Treat*. 2020;52:830-847. https://doi.org/10.4143/crt.2019.510.
32 Daher C, Vimeux L, Stoeva R, et al. Blockade of β-adrenergic receptors improves CD8(+) T-cell priming and cancer vaccine efficacy. *Cancer Immunol Res*. 2019;7:1849-1863. https://doi.org/10.1158/2326-6066.CIR-18-0833.
33 Falcinelli M, Al-Hity G, Baron S, et al. Propranolol reduces IFN-γ-driven PD-L1 immunosuppression and improves anti-tumour immunity in ovarian cancer. *Brain Behav Immun*. 2023;110:1-12. https://doi.org/10.1016/j.bbi.2023.02.011.
34 Huang M, Lu JJ, Ding J. Natural products in cancer therapy: past, present and future. *Nat Prod Bioprospect*. 2021;11:5-13. https://doi.org/10.1007/s13659-020-00293-7.
35 Wu Y, Pi D, Zhou S, et al. Ginsenoside Rh3 induces pyroptosis and ferroptosis through the STAT3/p53/NRF2 axis in colorectal cancer cells. *Acta Biochim Biophys Sin*. 2023;55:587-600. https://doi.org/10.3724/abbs.2023068.
36 Wu Y, Liang Y, Cui J, et al. Xiaoyao San reverses the pro-breast cancer effect of depression by inhibiting glutamate levels in intestinal flora. *J Ethnopharmacol*. 2026;355(Pt A):120636. https://doi.org/10.1016/j.jep.2025.120636.
37 Jennings A, Thompson AS, Tresserra-Rimbau A, et al. Flavonoid-rich foods, dementia risk, and interactions with genetic risk, hypertension, and depression. *JAMA Network Open*. 2024;7:e2434136. https://doi.org/10.1001/jamanetworkopen.2024.34136.
38 Samad N, Saleem A. Administration of *Allium cepa* L. bulb attenuates stress-produced anxiety and depression and improves memory in male mice. *Metab Brain Dis*. 2018;33:271-281. https://doi.org/10.1007/s11011-017-0159-1.
39 Rijnaarts I, Witteman B, Zoetendal EG, et al. Subtypes and severity of irritable bowel syndrome are not related to patients' self-reported dietary triggers: results from an online survey in Dutch adults. *J Acad Nutr Diet*. 2021;121:1750-1762. https://doi.org/10.1016/j.jand.2021.01.007.
40 Wu Y, Zhou S, Pi D, et al. Deciphering the molecular mechanism of Yifei-Sanjie Pill in cancer-related fatigue. *J Oncol*. 2023;2023:5486017. https://doi.org/10.1155/2023/5486017.
41 Wu Y, Pi D, Zhou S, et al. Yiqi Chutan Formula reverses cisplatin-induced apoptosis and ferroptosis of skeletal muscle by alleviating oxidative stress. *Integr Cancer Ther*. 2023;22:1563487253. https://doi.org/10.1177/15347354231172117.
42 Wu Y, Wang H, Liang Z, et al. Elucidating the mechanism of traditional Chinese medicine formula (Yifei-sanjie Pill) in alleviating the chemobrain based on network pharmacology and experimental verification. *J Tradit Complement Med*. 2024;16(1):17-30. https://doi.org/10.1016/j.jtcme.2024.11.008.